Chemical Engineering Journal 472 (2023) 145145

Contents lists available at ScienceDirect

Chemical Engineering Journal

journal homepage: www.elsevier.com/locate/cej

Methyl-functionalized flexible ultra-microporous MOF for efficient SF_6/N_2 mixture separation

Le Yan, Hui-Ting Zheng, Liang Song, Zhang-Wen Wei, Ji-Jun Jiang *, Cheng-Yong Su

Institute of Green Chemistry and Molecular Engineering, MOE Laboratory of Bioinorganic and Synthetic Chemistry, Lehn Institute of Functional Materials, School of Chemistry, Sun Yat-sen University, Guangzhou 510275, China

ARTICLE INFO

Keywords:
Metal-organic frameworks
Methyl functional
Gas adsorption
Breakthrough
SF_6/N_2 separation

ABSTRACT

In the semiconductor industry, SF_6/N_2 mixtures must be properly disposed of to protect the environment. Herein, three metal–organic frameworks with densely methyl-functionalized pores were designed to capture SF_6. Among them, $Zn(TMBDC)(DABCO)_{0.5}$ had the most suitable channels with the absorption capacity of 4.61 mmol/g, and the highest SF_6/N_2 selectivity is 239 at 298 K and 1 bar. Theoretical calculations indicated that introducing methyl groups provided more affinity sites that could bind SF_6. Cyclic breakthrough experiments confirmed the ability to directly separate SF_6 from a SF_6/N_2 mixture. This porous coordination network provides a method to construct other MOFs to separate SF_6/N_2 mixtures and other fluorinated gases.

1. Introduction

Due to its excellent dielectric and arc-quenching properties, sulfur hexafluoride (SF_6) [1] has been widely used in the power and semiconductor industries. SF_6 is an ideal etching agent used during electronics manufacturing, whose insulating performance is much better than that of other air-insulating media. [2] However, SF_6 is the most powerful greenhouse gas identified by the Kyoto Protocol, with a global warming potential 23900 times greater than that of CO_2 and an estimated atmospheric residence time of up to 3200 years. [3–6] Pure SF_6 cannot be directly used in actual production because it is expensive. Therefore, researchers have mixed it with N_2 gas to reduce the price and boiling point of SF_6. [7] However, most SF_6 remains intact after etching and must be decomposed via combustion, during which a small amount of the mixture is released into the atmosphere. Thus, a separation technology is needed to treat residual SF_6 in mixed gases. [5,8,9].

(Fig. 1) Current technical solutions such as low-temperature distillation, [10,11] adsorption, and membrane separation [12,13] provide sub-optimal performance due to the low SF_6 content in mixed waste gas. In recent years, pressure swing adsorption has been used in gas separation due to its simple operation and low energy consumption. Carbonaceous [14,15] or zeolite [16–19] adsorbents have poor separation efficiency and adsorption. For example, Zeolite-13X can only absorb 1.96 mmol/g of SF_6 under 1.0 bar with a maximum selectivity of only 56.5 (SF_6: N_2 = 1: 9).

Metal-organic frameworks (MOFs) [20–23] have a high Brunauer-Emmett-Teller (BET) specific surface area size and large pore volume, but they show a trade-off between their adsorption capacity and gas selectivity. MOFs with large pores tend to exhibit high maximum adsorption capacities for SF_6 but a low selectivity. For example, UiO-67 can adsorb 4.02 mmol/g SF_6 at 298 K and 1 bar, but it has a very low ideal adsorption solution theory (IAST) selectivity towards SF_6/N_2 gas mixtures of 21.6. [24] Microporous MOFs strongly interact with SF_6. For example, UiO-66-Br_2 had a high IAST selectivity of 220, but the adsorbed amount of SF_6 at 298 K and 1 bar was only 0.93 mmol/g. [25] Consequently, designing MOFs with high SF_6 adsorption capacity and high SF_6/N_2 selectivity remains challenging. Past studies have indicated that pore size is particularly important for capturing SF_6, so obtaining richly-functionalized MOFs with a suitable pore size is crucial. [26,27].

In this study, we employed a MOF, $Zn(BDC)(DABCO)_{0.5}$,(BDC = terephthalic acid, DABCO = 1,4-diazabicyclo[2.2.2]octane) as a prototype host material. Methyl-functionalized pores were constructed by replacing the BDC ligand with DMBDC and TMBDC ligands (DMBDC = 2,5-dimethyl-1,4-benzenedicarboxylic acid, TMBDC = 2,3,5,6-tetramethylterephthalic acid) in the $Zn(BDC)(DABCO)_{0.5}$ framework. Through this strategy, we obtained $Zn(DMBDC)(DABCO)_{0.5}$ and $Zn(TMBDC)(DABCO)_{0.5}$ with similar frameworks to $Zn(BDC)(DABCO)_{0.5}$. The variation of the IAST selectivity of SF_6/N_2 shows that the introduction of different amounts of methyl groups into the MOF can effectively improve the separation performance of SF_6/N_2. After introducing

* Corresponding author.
E-mail address: jiangjij@mail.sysu.edu.cn (J.-J. Jiang).

https://doi.org/10.1016/j.cej.2023.145145
Received 15 May 2023; Received in revised form 20 July 2023; Accepted 29 July 2023
Available online 1 August 2023

DMBDC and TMBDC, the MOFs exhibited different SF_6/N_2 adsorption performances. Transient breakthrough experiments further confirmed the ability to directly separate SF_6 from a simulated gas mixture.

2. Experimental section

Synthesis of Zn(BDC)(DABCO)$_{0.5}$. Zn(BDC)(DABCO)$_{0.5}$ was prepared according to previous reports using a solvothermal method. [28] Zn$(NO_3)_2{\cdot}6H_2O$ (0.245 g, 0.82 mmol), H_2BDC (0.136 g, 0.97 mmol), and DABCO (0.073 g, 0.65 mmol) were mixed in DMF (15 mL). The solution was then transferred to a Teflon-lined stainless-steel autoclave and heated at 120 °C for 48h. When the autoclave was cooled to room temperature, colorless crystals were collected by centrifugation (10 000 rpm, 5 min) and washed with DMF and ethanol several times. Samples of Zn(BDC)(DABCO)$_{0.5}$ were activated by heating the as-synthesized materials at 100 °C for 12h in a degasser.

Synthesis of Zn(DMBDC)(DABCO)$_{0.5}$. Zn(DMBDC)(DABCO)$_{0.5}$ was prepared similarly to Zn(BDC)(DABCO)$_{0.5}$. [28] Zn$(NO_3)_2{\cdot}6H_2O$ (0.189 g, 0.635 mmol), DMBDC (0.122 g, 0.628 mmol), and DABCO (0.035 g, 0.31 mmol) were mixed in DMF (15 mL, 828.12 mmol). All other steps were the same as above.

Synthesis of Zn(TMBDC)(DABCO)$_{0.5}$. Zn(TMBDC)(DABCO)$_{0.5}$ was prepared similarly to Zn(BDC)(DABCO)$_{0.5}$ and Zn(DMBDC)(DABCO)$_{0.5}$. [28] Zn$(NO_3)_2{\cdot}6H_2O$ (0.189 g, 0.635 mmol), TMBDC (0.140 g, 0.630 mmol), and DABCO (0.035 g, 0.31 mmol) were mixed in DMF (15 mL, 828.12 mmol). All other steps were the same as above.

3. Results and discussion

All three MOFs were prepared according to previous reports using a solvothermal method. The pillar-layered Zn(BDC)(DABCO)$_{0.5}$ is connected by a zinc paddlewheel with four linear connectors of BDC to form a two-dimensional regular square layer, and the DABCO pillar-layer forms a 3D framework. Zn(BDC)(DABCO)$_{0.5}$ shows a 6-coordinate network with ***PCU*** topology. Zn(DMBDC)(DABCO)$_{0.5}$ and Zn(TMBDC)(DABCO)$_{0.5}$ are isomorphic to Zn(BDC)(DABCO)$_{0.5}$. The powder X-ray diffraction (PXRD) patterns of the three MOFs matched well with the simulated patterns (Fig. S1–S3), confirming the phase purity of the bulk samples. Thermogravimetric analysis (TGA) and variable-temperature PXRD experiments were performed to investigate the thermal stability of the three MOFs (Fig. S4–S7). The results showed that Zn(BDC)(DABCO)$_{0.5}$ and Zn(DMBDC)(DABCO)$_{0.5}$ were stable until 275 °C and 200 °C, while Zn(TMBDC)(DABCO)$_{0.5}$ remained stable until 325 °C. FT-IR spectra were recorded to confirm the synthesis of the MOFs (Fig. S8). The spectra of all three MOFs showed an absorption band at 1055 cm^{-1}, which corresponded to the vibrations of the NC_3 group in the DABCO pillar ligand means that DABCO is synthesized into the structure of the MOF [29–32]. The result of infrared spectra further proves the success of MOF synthesis.

N_2 adsorption experiments at 77 K were used to evaluate the sample's surface area and porosity (Fig. 2a and Figs. S9 – S11). All three materials exhibited typical type-I sorption isotherms, suggesting the frameworks were microporous. The BET surface areas of Zn(BDC)(DABCO)$_{0.5}$, Zn(DMBDC)(DABCO)$_{0.5}$, and Zn(TMBDC)(DABCO)$_{0.5}$ were 1978.1, 1336.1, and 975.9 m^2/g, respectively, which correspond to pore volumes of 0.79, 0.56, and 0.42 $cm^3\ g^{-1}$. Decreases in both the BET surface area and accessible pore volume were ascribed to the higher ratio of methyl groups in the framework. Based on nonlinear density functional theory (NLDFT), pore-size distributions were calculated to be 7.8 Å for Zn(BDC)(DABCO)$_{0.5}$, 6.7 Å for Zn(DMBDC)(DABCO)$_{0.5}$, and 5.4 Å for Zn(TMBDC)(DABCO)$_{0.5}$ (Fig. 2b and Table S1). The kinetic diameter of SF_6 is 5.2 Å which is close to the pore size of Zn(TMBDC)(DABCO)$_{0.5}$, which suggests that Zn(TMBDC)(DABCO)$_{0.5}$ may strongly interact with SF_6.

The SF_6 and N_2 adsorption isotherms of all three MOFs at 273/298 K and 1 bar were collected to evaluate their uptake capacities. When the temperature increased from 273 K to 298 K, the adsorption amounts of all three gases declined, indicating that physisorption occurred on the MOFs. Despite having the highest specific surface area, Zn(BDC)(DABCO)$_{0.5}$ showed the lowest uptake of SF_6 (3.48 mmol/g) and N_2 (0.17 mmol/g) at 100 kPa and 298 K due to the lack of functional sites and larger pore size. At 298 K and 1 bar, Zn(DMBDC)(DABCO)$_{0.5}$ adsorbed 4.77 mmol/g SF_6, which was significantly higher than that of Zn(BDC)(DABCO)$_{0.5}$ because of the introduction of methyl groups. Even though Zn(TMBDC)(DABCO)$_{0.5}$ adsorbed 4.61 mmol/g SF_6, which was almost the same as that of Zn(DMBDC)(DABCO)$_{0.5}$ at 273/298 K and 1 bar, the SF_6 adsorption capacity of Zn(TMBDC)(DABCO)$_{0.5}$ at 0.1 bar (low pressure) was 2.48 mmol/g, which was higher than that of Zn(BDC)(DABCO)$_{0.5}$ (0.57 mmol/g) and Zn(DMBDC)(DABCO)$_{0.5}$ (1.40 mmol/g). This value was also higher than that of many reported MOFs, including UiO-66-Br_2 (0.75 mmol/g), [25] SBMOF-1 (0.93 mmol/g), [33] Ni$(ina)_2$ (2.39 mmol/g), [27] Mg-MOF-74 (2.1 mmol/g), [34] Zn-MOF-74 (1.35 mmol/g), [34] $Im_{1\%}$@HKUST-1 (1.25 mmol/g), [35] UiO-66 (0.82 mmol/g), [24] UiO-67 (0.4 mmol/g), [24] HKUST-1c (1.32 mmol/g), [36] Ni(adc)(dabco)$_{0.5}$[26], and DUT-9 (0.80 mmol/g).[37] As a result, Zn(TMBDC)(DABCO)$_{0.5}$ showed excellent performance at low pressures, suggesting that its highly methyl-functionalized pores were suitable for capturing SF_6. The SF_6 adsorption by Zn(DMBDC)(DABCO)$_{0.5}$ and Zn(TMBDC)(DABCO)$_{0.5}$ was maintained after five SF_6 adsorption–desorption cycles, as depicted in Fig. 3e and 3f. Notably, the two-step isotherms of SF_6 revealed threshold pressures of 0.64 bar and 0.78 bar for Zn(DMBDC)(DABCO)$_{0.5}$ and Zn(TMBDC)(DABCO)$_{0.5}$. This is the first time a MOF has exhibited a pore-opening phenomenon during SF_6 adsorption. We have subsequently verified this phenomenon by

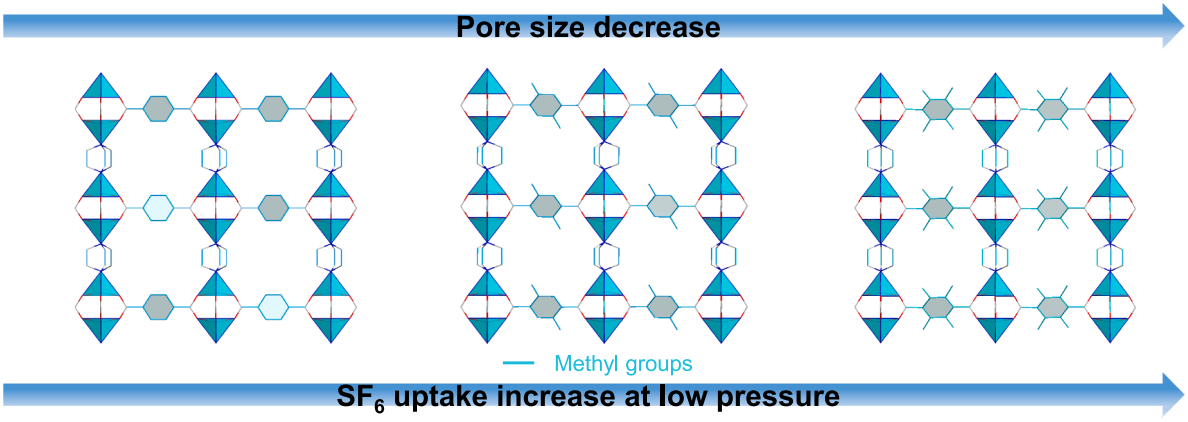

Fig. 1. Structural illustration of synthesized Zn(BDC)(DABCO)$_{0.5}$, Zn(DMBDC)(DABCO)$_{0.5}$, and Zn(TMBDC)(DABCO)$_{0.5}$ upon increasing the number of methyl groups.

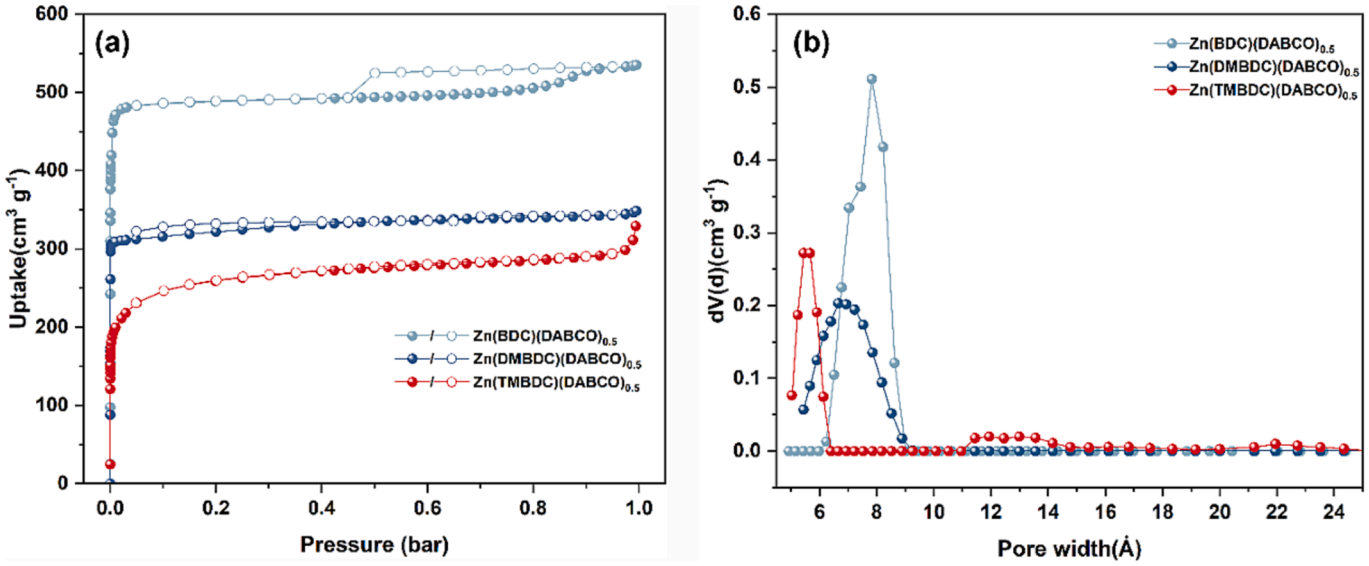

Fig. 2. (a) N_2 adsorption isotherms of Zn(BDC)(DABCO)$_{0.5}$, Zn(DMBDC)(DABCO)$_{0.5}$, and Zn(TMBDC)(DABCO)$_{0.5}$ at 77 K. Solid symbols: adsorption; open symbols: desorption. (b) Pore size distribution of Zn(BDC)(DABCO)$_{0.5}$, Zn(DMBDC)(DABCO)$_{0.5}$, and Zn(TMBDC)(DABCO)$_{0.5}$ calculated using the QSDFT module.

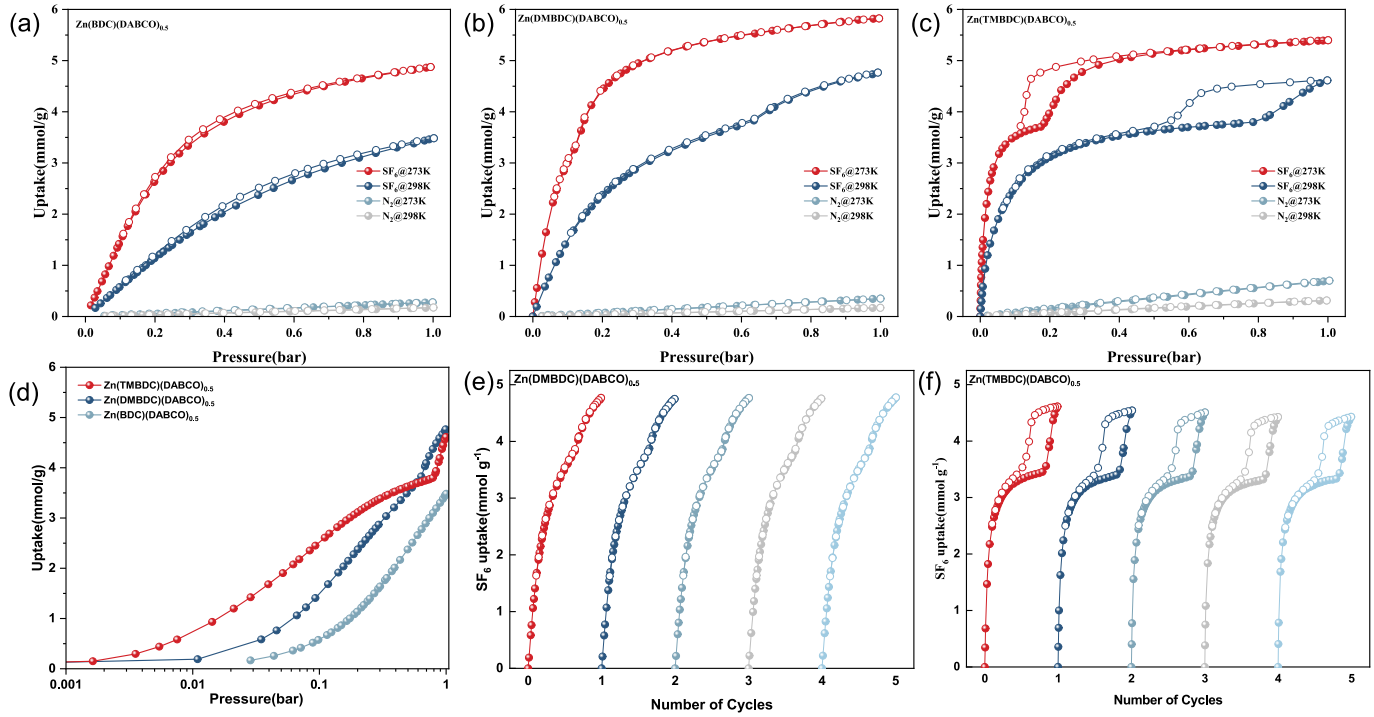

Fig. 3. SF_6 and N_2 sorption isotherms for (a) Zn(BDC)(DABCO)$_{0.5}$, (b) Zn(DMBDC)(DABCO)$_{0.5}$, and (c) Zn(TMBDC)(DABCO)$_{0.5}$ at 273 K and 298 K.(d) The enlarged SF_6 adsorption at low pressure of 0.001–1 bar for better clarity of the different adsorption performance of the three MOFs. (e) Cyclic regeneration tests on Zn (DMBDC)(DABCO)$_{0.5}$ and (f) Zn(TMBDC)(DABCO)$_{0.5}$ toward SF_6.

powder diffraction, but unfortunately, no clear evidence has been obtained. As shown in Fig. S12, there is little difference between the PXRD patterns of MOFs loading SF_6 and the patterns of as-synthesized MOFs. We speculated that the change of structure which caused by the rotation of linker ligand is too small to observe in in-situ XRD. Some similar results also have been reported before. [38 39] Besides, single-crystal of Zn (DMBDC)(DABCO)$_{0.5}$ was obtained successfully. Unfortunately, the crystal loading SF_6 were damaged so that the single crystal structure could not be obtained (Fig. S13). We speculate that the gate-opening phenomenon was associated with extra tilting of the flexible benzene ring under SF_6 gas stimuli. [40–44].

Additionally, the isosteric heat of adsorption (Q_{st}) was applied to evaluate the energetic heterogeneity of the adsorbent surface and the interactions between adsorbents and adsorbates. Herein, we calculated the Q_{st} of N_2 and SF_6 for the three MOFs based on adsorption isotherms at 273 K and 298 K using the Clausius-Clapeyron equation. At zero coverage, the Q_{st} value of SF_6 for Zn(TMBDC)(DABCO)$_{0.5}$ was 45.2 kJ/mol, which was higher than that for N_2 (24.6 kJ/mol). Besides, the Q_{st} value of SF_6 for Zn(TMBDC)(DABCO)$_{0.5}$ was much higher than that of Ni (ina)$_2$ (33.4), [27] CAU-17(33.0) [45], and SBMOF-1(32.5). [33] For all three MOFs, the Q_{st} of SF_6 was greater than that of N_2 adsorption, indicating that interactions of SF_6 with the three MOFs were stronger

than those of N_2. The obtained Q_{st} value of SF_6 for Zn(BDC)(DABCO)$_{0.5}$ was 23.2 kJ/mol, which was lower than those of Zn(DMBDC)(DABCO)$_{0.5}$ (29.7 kJ/mol) and Zn(TMBDC)(DABCO)$_{0.5}$. (Fig. 4a and Figs. S14-S19) This was consistent with its lower gas uptake.

The adsorption selectivity of Zn(BDC)(DABCO)$_{0.5}$, Zn(DMBDC)(DABCO)$_{0.5}$, and Zn(TMBDC)(DABCO)$_{0.5}$ at 298 K and 1 bar was calculated using the ideal adsorption solution theory (IAST). Fig. 4b shows the IAST-predicted selectivity of SF_6/N_2 ($SF_6/N_2 = 1/9$) mixtures by the three MOFs. The predicted selectivity of SF_6/N_2 for Zn(TMBDC)(DABCO)$_{0.5}$ reached 239, which was higher than that of most reported MOFs, including HKUST-1 (70.4), [36] UiO-66 (127.8), [24] UiO-66-Br_2 (220.0), [25]CAU-17 (31.0), [45] MOF-74(Zn) (46.0), [34] MOF-74(Co) (40), [34] MOF-74(Mg) (32.0), [34] MIL-100(Fe) granule (25), [46] UiO-67 (21.6) [24], and MIL-100(Fe) (24.4). The IAST-predicted SF_6/N_2 ($SF_6/N_2 = 1/9$) selectivities of Zn(BDC)(DABCO)$_{0.5}$ and Zn(DMBDC)(DABCO)$_{0.5}$ reached 31.8 and 118.9 at 298 K and 1 bar, respectively. Zn(DMBDC)(DABCO)$_{0.5}$ had the highest adsorption capacity at 298 K and 1 bar, and its selectivity was moderate compared with previously-reported MOFs. Zn(DMBDC)(DABCO)$_{0.5}$ and Zn(TMBDC)(DABCO)$_{0.5}$ both showed SF_6/N_2 selectivity and remarkable SF_6 uptake capacities due to the introduction of methyl groups. (Fig. 4b and Table S2)

To better understand host–guest binding interactions, Grand Canonical Monte Carlo (GCMC) calculations were used to calculate the adsorption density distributions, adsorption binding sites, and simulated Q_{st} values for SF_6 within the three MOFs. (See the **Supporting Information** for details). The density distribution map of Zn(BDC)(DABCO)$_{0.5}$ shows that SF_6 weakly interacted with the framework and was highly distributed throughout the pores (Fig. S23). Nevertheless, DABCO contained more H atoms and was more attractive to the gas than the phenyl ring. For Zn(DMBDC)(DABCO)$_{0.5}$, SF_6 was primarily located close to both DABCO and methyl groups. The high methyl group density of Zn(TMBDC)(DABCO)$_{0.5}$ produced very small pores, so SF_6 could only stay in the remaining spaces. As expected, SF_6 also preferred to interact with the methyl group and DABCO. Adsorption location calculations also provided the same results for the primary adsorption sites. For Zn(BDC)(DABCO)$_{0.5}$, F atoms in the direction of the benzene ring exhibited multiple –F···H– bond lengths (2.989–3.039Å) with the hydrogen atoms of the MOF pyridine ring. The F atom close to the DABCO was more likely to form a –F···H– bond (2.782–3.605Å) with the H atom of DABCO (Fig. 5a). Compared with Zn(BDC)(DABCO)$_{0.5}$, the F atom simultaneously interacted with the H atom in different positions (–F···H–(benzene ring) (3.145–3.188 Å), –F···H–(DABCO) (2.457–3.360 Å), and –F···H–(methyl group) (2.749–3.369 Å)) in Zn(DMBDC)(DABCO)$_{0.5}$ (Fig. 5b). Interestingly, the benzene ring rotated after introducing the methyl group, moving the F atom closer to the center of the benzene ring. The F atom near the benzene ring cooperated with the host framework via F···π interactions (3.343–3.945 Å). For SF_6 in Zn(TMBDC)(DABCO)$_{0.5}$, the preferential adsorption sites were roughly the same as those of Zn(DMBDC)(DABCO)$_{0.5}$. The methyl group loaded in the pores provided H sites and also constricted the pores. SF_6 was fixed through 12 -F···H-(DABCO) bonds (2.763–3.295 Å) in the framework (Fig. 5c). These results confirm that the introduction of methyl groups changed the host–guest interactions. Correspondingly, the calculated Q_{st} at this site followed the order Zn(TMBDC)(DABCO)0.5 (45.1 kJ/mol) > Zn(DMBDC)(DABCO)0.5 (26.5 kJ/mol) > Zn(BDC)(DABCO)0.5 (23.2 kJ/mol) (Table S3). The trend of theoretical binding energies closely matched that of the experimental Q_{st} values at zero coverage.

We conducted multi-cycle dynamic penetration experiments on three MOFs using a laboratory-scale penetration apparatus to evaluate the practical separation performance of SF_6/N_2 mixtures. The SF_6/N_2 gas mixture (1/9) was flowed through a packed column of activated MOF samples. For Zn(TMBDC)(DABCO)$_{0.5}$, N_2 rapidly breaks through the column. In comparison, the penetration time of SF_6 is 3900 s g^{-1}, which is longer than that of Zn(DMBDC)(DABCO)$_{0.5}$ (1200 s g^{-1}). Among these materials, Zn(BDC)(DABCO)$_{0.5}$ has the shortest SF_6 breakthrough time (600 s g^{-1}), further demonstrating the feasibility of using methyl modification to improve the separation of SF_6/N_2 mixtures. Mass spectrometer is greatly affected by environmental noise, which will cause the fluctuation of N_2 signal. In addition, more attention is paid to the penetration time of N_2 and SF_6 in the experiment, and the fluctuation of N_2 signal has little effect on the experimental results. Zn(TMBDC)(DABCO)$_{0.5}$ can capture 1.53 mol/kg of SF_6, while the calculated SF_6 values of Zn(DMBDC)(DABCO)$_{0.5}$ and Zn (BDC) (DABCO)$_{0.5}$ are 0.65 mol/kg and 0.29 mol/kg, respectively. [47] (Fig. 6(a-c)). To evaluate the regeneration potential of the two methyl-functional MOFs, a packed column was flowed at a rate of 5 mL min^{-1} at 80 °C. As shown in Fig. S20, Zn(TMBDC)(DABCO)$_{0.5}$ can be fully activated after 202 min/g, which is longer than Zn(DMBDC)(DABCO)$_{0.5}$ (59 min/g), indicating that our material has good regeneration ability. In the desorption experiment after breakthrough, for Zn(TMBDC)(DABCO)$_{0.5}$ (99.6%) and Zn(TMBDC)(DABCO)$_{0.5}$ (99.6%), high grade SF_6 can be obtained after N_2 is completely eluted. We also performed cyclic penetration experiments to assess potential practical applications. As shown in Fig. 6(d-f), the breakthrough time of all three MOFs remained almost unchanged, confirming that MOFs are promising adsorbents with good regeneration and cycling performance. After the cycling breakthrough experiment, the PXRD patterns of all three materials remained almost unchanged (Fig. S21), indicating their cycling stability.

4. Conclusion

In summary, we reported a series of Zn-based MOFs for separating SF_6/N_2 mixtures. Compared with Zn(BDC)(DABCO)$_{0.5}$ and Zn(DMBDC)(DABCO)$_{0.5}$, Zn(TMBDC)(DABCO)$_{0.5}$ presented the highest SF_6 adsorption and SF_6/N_2 selectivity at a low pressure. It showed a trade-off between adsorption capacity and gas selectivity because its micropores were densely functionalized with methyl groups. Its performance exceeded that of most previously-reported materials. Zn(DMBDC)

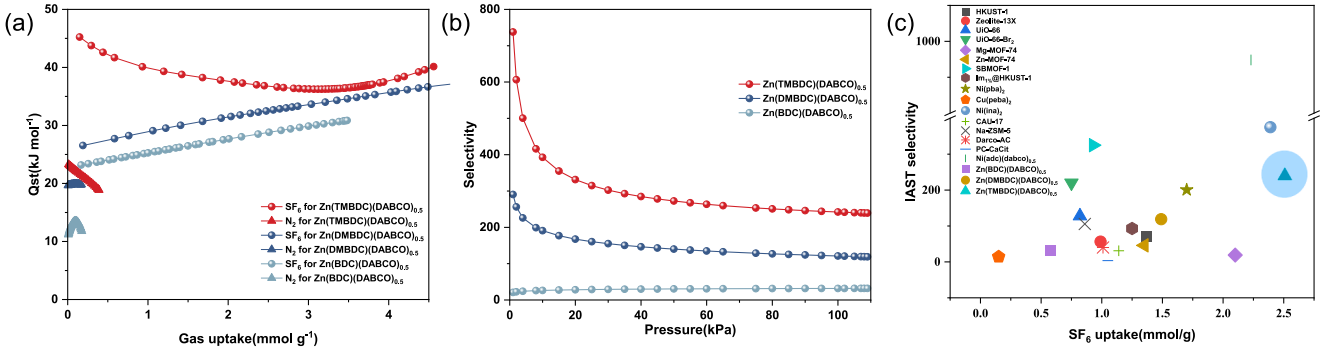

Fig. 4. (a) Q_{st} of SF_6 and N_2 adsorption by the MOFs as a function of the surface coverage. (b) IAST selectivity of the MOFs. (c) Comparison of ideal selectivity and SF_6 uptakes at 298 K and 0.1 bar in Zn(BDC)(DABCO)$_{0.5}$, Zn(DMBDC)(DABCO)$_{0.5}$, Zn(TMBDC)(DABCO)$_{0.5}$, and other previously-reported adsorbents.

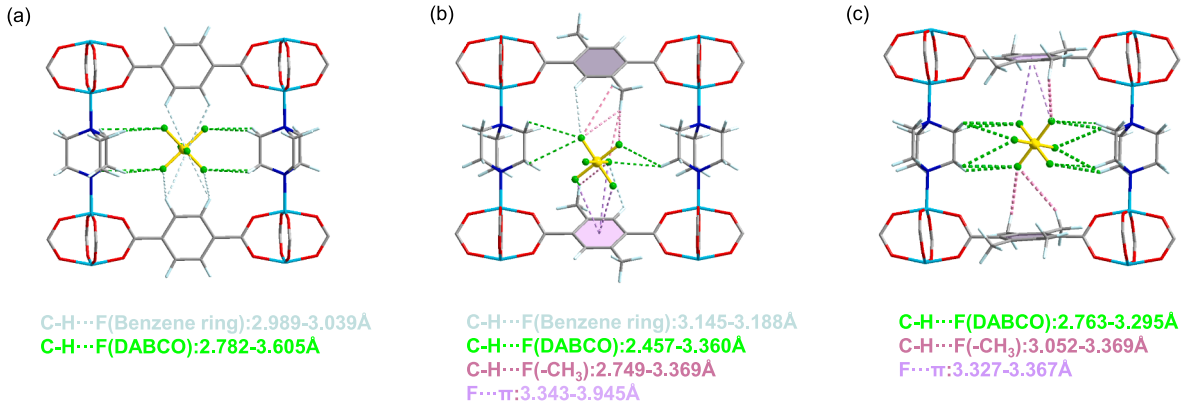

Fig. 5. Primary adsorption sites of SF_6 within (a) Zn(BDC)(DABCO)$_{0.5}$, (b) Zn(DMBDC)(DABCO)$_{0.5}$, and (c) Zn(TMBDC)(DABCO)$_{0.5}$.

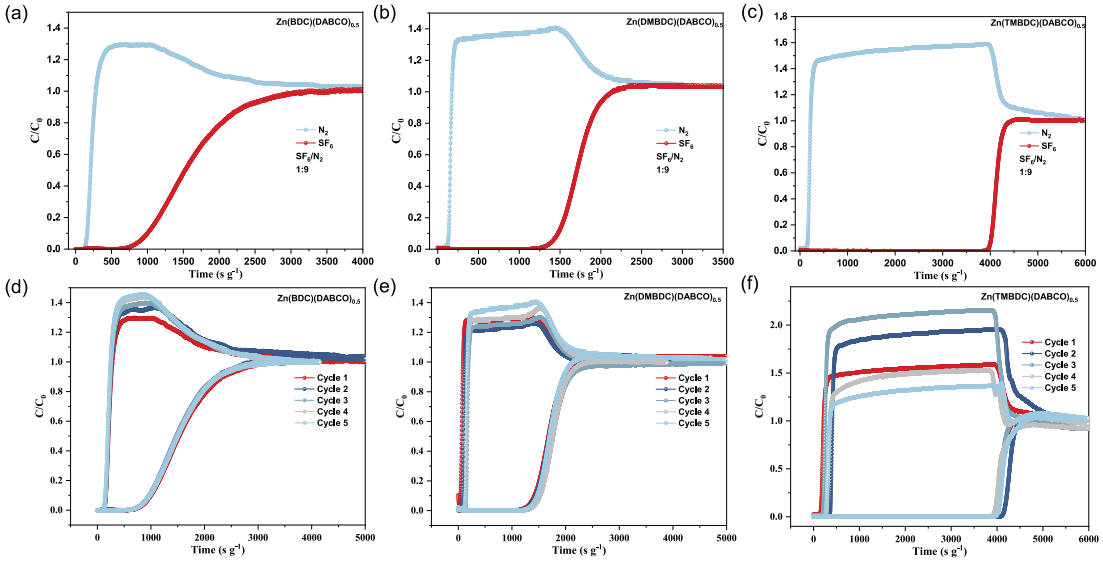

Fig. 6. Breakthrough curves of (a) Zn(BDC)(DABCO)$_{0.5}$, (b) Zn(DMBDC)(DABCO)$_{0.5}$, and (c) Zn(TMBDC)(DABCO)$_{0.5}$ for separating a SF_6/N_2 (1:9, v:v) mixture. Cyclic column breakthrough curves of (d) Zn(BDC)(DABCO)$_{0.5}$, (e) Zn(DMBDC)(DABCO)$_{0.5}$ and (f) Zn(TMBDC)(DABCO)$_{0.5}$ for SF_6/N_2 (1/9, v/v) mixture.

(DABCO)$_{0.5}$ and Zn(TMBDC)(DABCO)$_{0.5}$ exhibited stepped adsorption isotherms due to their flexible structures. Theoretical calculations showed that SF_6 more strongly interacted with the framework via methyl groups in its channels. Cyclic breakthrough experiments confirmed that real SF_6/N_2 mixtures could be separated using Zn (TMBDC)(DABCO)$_{0.5}$ due to strong binding forces between its methyl groups and the F atoms of SF_6. This suggests it can be applied to capture other plasma etching gas such as CF_4 and NF_3. This work may help design ultra-microporous MOFs modified with various functional groups to adsorb and separate other greenhouse gases.

Declaration of Competing Interest

The authors declare that they have no known competing financial interests or personal relationships that could have appeared to influence the work reported in this paper.

Data availability

I have shared the link to my data/code at the Attach file steps

Acknowledgements

We acknowledge financial support from the research was supported by the NKRD Program of China (2021YFA1500401), the National Natural Science Foundation of China (Grants 21821003, 21890380), Local Innovative and Research Teams Project of.

Guangdong Pearl River Talents Program (Grant 2017BT01C161), and Fundamental Research Funds for the Central Universities.

Appendix A. Supplementary data

Supplementary data to this article can be found online at https://doi.org/10.1016/j.cej.2023.145145.

References

[1]] Rigby M, Mühle J, Miller B R, Prinn R G, Krummel P B, Steele L P, Fraser P J, Salameh P K, Harth C M, Weiss R F, Greally B R, O'doherty S, Simmonds P G, Vollmer M K, Reimann S, Kim J, Kim K R, Wang H J, Olivier J G J, Dlugokencky E J, Dutton G S, Hall B D, Elkins J W. History of atmospheric SF_6 from 1973 to 2008 . *Atmos. Chem. Phys.*, **2010**, *10* (21): 10305-20.

[2] F. Illuzzi, H. Thewissen, Perfluorocompounds emission reduction by the semiconductor industry, J. Integr. Environ. Sci. 7 (sup1) (2010) 201–210.

[3] X. Fang, X. Hu, G. Janssens-Maenhout, J. Wu, J. Han, S. Su, J. Zhang, J. Hu, Sulfur Hexafluoride (SF_6) Emission Estimates for China: An Inventory for 1990–2010 and a Projection to 2020, Environ. Sci. Technol. 47 (8) (2013) 3848–3855.

[4] A.R. Ravishankara, S. Solomon, A.A. Turnipseed, R.F. Warren, Atmospheric Lifetimes of Long-Lived Halogenated Species, Science 259 (5092) (1993) 194–199.

[5] W.T. Tsai, The decomposition products of sulfur hexafluoride (SF_6): Reviews of environmental and health risk analysis, J. Fluorine Chem. 128 (11) (2007) 1345–1352.

[6] L.G. Christophorou, R.J.V. Brunt, SF_6/N_2/ mixtures: basic and HV insulation properties, IEEE Trans. Dielectr. Electr. Insul. 2 (5) (1995) 952–1003.

[7] E.K. Lee, J.D. Lee, H.J. Lee, B.R. Lee, Y.S. Lee, S.M. Kim, H.O. Park, Y.S. Kim, Y.-D. Park, Y.D. Kim, Pure SF_6 and SF_6-N_2 Mixture Gas Hydrates Equilibrium and Kinetic Characteristics, Environ. Sci. Technol. 43 (20) (2009) 7723–7727.

[8] P.S. Lee, M.S. Lim, A. Park, H. Park, S.-E. Nam, Y.-I. Park, A zeolite membrane module composed of SAPO-34 hollow fibers for use in fluorinated gas enrichment, J. Membr. Sci. 542 (2017) 123–132.

[9] M.B. Chang, J.-S. Chang, Abatement of PFCs from Semiconductor Manufacturing Processes by Nonthermal Plasma Technologies: A Critical Review, Ind. Eng. Chem. Res. 45 (12) (2006) 4101–4109.

[10] C.Y. Chuah, W. Li, S.A.S.C. Samarasinghe, G.S.M.D.P. Sethunga, T.-H. Bae, Enhancing the CO_2 separation performance of polymer membranes via the incorporation of amine-functionalized HKUST-1 nanocrystals, Microporous Mesoporous Mater. 290 (2019) 109680.

[11] Xu G, Liang F, Yang Y, Hu Y, Zhang K, Liu W. An Improved CO_2 Separation and Purification System Based on Cryogenic Separation and Distillation Theory [J/OL] 2014, 7(5):3484-502[10.3390/en7053484.

[12] C.Y. Chuah, Y. Lee, T.-H. Bae, Potential of adsorbents and membranes for SF_6 capture and recovery: A review, Chem. Eng. J. 404 (2021) 126577.

[13] A. Wolińska-Grabczyk, A. Jankowski, R. Sekuła, B. Kruczek, Separation of SF_6 from Binary Mixtures with N_2 Using Commercial Poly(4-Methyl-1-Pentene) Films, Sep. Sci. Technol. 46 (8) (2011) 1231–1240.

[14] I. Skarmoutsos, E.N. Koukaras, C. Galiotis, G.E. Froudakis, E. Klontzas, Porous carbon nanotube networks and pillared graphene materials exhibiting high SF_6 adsorption uptake and separation selectivity of SF_6/N_2 fluid mixtures: A comparative molecular simulation study, Microporous Mesoporous Mater. 307 (2020) 110464.

[15] A. Takase, H. Kanoh, T. Ohba, Wide Carbon Nanopores as Efficient Sites for the Separation of SF_6 from N_2, Sci. Rep. (2015) 5.

[16] D.V. Cao, S. Sircar, Heat of adsorption of pure sulfur hexafluoride on micro-mesoporous adsorbents, Adsorpt.-J. Int. Adsorpt. Soc. 7 (1) (2001) 73–80.

[17] S. Chen, Y. Shen, Z. Guan, B. Liu, Z. Tang, D. Zhang, B. Fu, Adsorption Properties of SF6 on Zeolite NaY, 13X, Activated Carbon, and Silica Gel, J. Chem. Eng. Data 65 (8) (2020) 4044–4051.

[18] W.S. Cho, K.H. Lee, H.J. Chang, W. Huh, H.H. Kwon, Evaluation of pressure-temperature swing adsorption for sulfur hexafluoride (SF_6) recovery from SF_6 and N_2 gas mixture, Korean J. Chem. Eng. 28 (11) (2011) 2196–2201.

[19] I. Matito-Martos, J. Álvarez-Ossorio, J.J. Gutiérrez-Sevillano, M. Doblaré, A. Martin-Calvo, S. Calero, Zeolites for the selective adsorption of sulfur hexafluoride, Phys. Chem. Chem. Phys. 17 (27) (2015) 18121–18130.

[20] B. Chen, M. Eddaoudi, S.T. Hyde, M. O'Keeffe, O.M. Yaghi, Interwoven Metal-Organic Framework on a Periodic Minimal Surface with Extra-Large Pores, Science 291 (5506) (2001) 1021–1023.

[21] S. Kitagawa, R. Kitaura, S. Noro, Functional porous coordination polymers, Angew. Chem. Int. Ed. 43 (18) (2004) 2334–2375.

[22] Wang Y X, Peh S B, Zhao D. Alternatives to Cryogenic Distillation: Advanced Porous Materials in Adsorptive Light Olefin/Paraffin Separations. *Small*, **2019**, *15* (25).

[23] D. Wanigarathna, J.J. Gao, B. Liu, Metal organic frameworks for adsorption-based separation of fluorocompounds: a review, Mater. Adv. 1 (3) (2020) 310–320.

[24] M.-B. Kim, T.-H. Kim, T.-U. Yoon, J.H. Kang, J.-H. Kim, Y.-S. Bae, Efficient SF_6/N_2 separation at high pressures using a zirconium-based mesoporous metal–organic framework, J. Ind. Eng. Chem. 84 (2020) 179–184.

[25] M.-B. Kim, K.-M. Kim, T.-H. Kim, T.-U. Yoon, E.-J. Kim, J.-H. Kim, Y.-S. Bae, Highly selective adsorption of SF_6 over N_2 in a bromine-functionalized zirconium-based metal-organic framework, Chem. Eng. J. 339 (2018) 223–229.

[26] M. Chang, T. Yan, Y. Wei, J.-X. Wang, D. Liu, J.-F. Chen, Metal-Organic Framework-Based Single-Molecule SF6 Trap for Record SF6 Capture, Chem. Mater. 34 (20) (2022) 9134–9143.

[27] S.M. Wang, X.T. Mu, H.R. Liu, S.T. Zheng, Q.Y. Yang, Pore-Structure Control in Metal-Organic Frameworks (MOFs) for Capture of the Greenhouse Gas SF_6 with Record Separation, Angew. Chem. Int. Ed. (2022) 61 (33).

[28] N.C. Burtch, H. Jasuja, D. Dubbeldam, K.S. Walton, Molecular-level Insight into Unusual Low Pressure CO2 Affinity in Pillared Metal-Organic Frameworks, J. Am. Chem. Soc. 135 (19) (2013) 7172–7180.

[29] K. Tan, P. Canepa, Q. Gong, J. Liu, D.H. Johnson, A. Dyevoich, P.K. Thallapally, T. Thonhauser, J. Li, Y.J. Chabal, Mechanism of Preferential Adsorption of SO2 into Two Microporous Paddle Wheel Frameworks M(bdc), Chem. Mater. 25 (23) (2013) 4653–4662.

[30] Marzocchi M P, Sbrana G, Zerbi G. Structure and Fundamental Vibrations of Cage Molecules. I. 1,4-Diazabicyclo[2.2.2]octane1 . *J. Am. Chem. Soc.*, **1965**, *87* (7): 1429-32.

[31] K. Tan, N. Nijem, P. Canepa, Q. Gong, J. Li, T. Thonhauser, Y.J. Chabal, Stability and Hydrolyzation of Metal Organic Frameworks with Paddle-Wheel SBUs upon Hydration, Chem. Mater. 24 (16) (2012) 3153–3167.

[32] J. Guerrero-Medina, G. Mass-González, L. Pacheco-Londoño, S.P. Hernández-Rivera, R. Fu, A.J. Hernández-Maldonado, Long and local range structural changes in M[(bdc)(ted)0.5] (M = Zn, Ni or Cu) metal organic frameworks upon spontaneous thermal dispersion of LiCl and adsorption of carbon dioxide, Microporous Mesoporous Mater. 212 (2015) 8–17.

[33] T. Wang, M. Chang, T. Yan, Y. Ying, Q. Yang, D. Liu, Calcium-Based Metal-Organic Framework for Efficient Capture of Sulfur Hexafluoride at Low Concentrations, Ind. Eng. Chem. Res. 60 (16) (2021) 5976–5983.

[34] M.B. Kim, S.J. Lee, C.Y. Lee, Y.S. Bae, High SF_6 selectivities and capacities in isostructural metal-organic frameworks with proper pore sizes and highly dense unsaturated metal sites, Microporous Mesoporous Mater. 190 (2014) 356–361.

[35] P. Liu, T. Zhao, K. Cai, P. Chen, F. Liu, D.-J. Tao, Rapid mechanochemical construction of HKUST-1 with enhancing water stability by hybrid ligands assembly strategy for efficient adsorption of SF6, Chem. Eng. J. 437 (2022) 135364.

[36] C.Y. Chuah, K. Goh, T.-H. Bae, Hierarchically Structured HKUST-1 Nanocrystals for Enhanced SF_6 Capture and Recovery, J. Phys. Chem. C 121 (12) (2017) 6748–6755.

[37] I. Senkovska, E. Barea, J.a.R. Navarro, S. Kaskel, Adsorptive capturing and storing greenhouse gases such as sulfur hexafluoride and carbon tetrafluoride using metal–organic frameworks, Microporous Mesoporous Mater. 156 (2012) 115–120.

[38] Q. Wang, T. Ke, L. Yang, Z. Zhang, X. Cui, Z. Bao, Q. Ren, Q. Yang, H. Xing, Separation of Xe from Kr with Record Selectivity and Productivity in Anion-Pillared Ultramicroporous Materials by Inverse Size-Sieving, Angew. Chem. Int. Ed. 59 (9) (2020) 3423–3428.

[39] J. Zhou, T. Ke, X. Zhu, B. Jin, Z. Bao, Z. Zhang, Y. Yang, Q. Ren, Q. Yang, Combination of Low-Polar and Polar Binding Sites in Aliphatic MOFs for the Efficient C2H6/C2H4 Separation, ACS Appl. Mater. Interfaces 15 (2) (2023) 3387–3394.

[40] B. Gao, Z. Zhang, J. Hu, J. Cui, L. Chen, X. Cui, H. Xing, Efficient separation of C4 olefins using tantalum pentafluor oxide anion-pillared hybrid microporous material, Chin. J. Chem. Eng. 42 (2022) 49–54.

[41] O. Saengsawang, V. Vchirawongkwin, T. Remsungnen, M. Wiebcke, S. Fritzsche, S. Hannongbua, Rotational flexibility of bridging ligands in paddle–wheel layer–pillar metal–organic frameworks studied by quantum calculations, Comput. Theor. Chem. 1001 (2012) 33–38.

[42] N.C. Burtch, A. Torres-Knoop, G.S. Foo, J. Leisen, C. Sievers, B. Ensing, D. Dubbeldam, K.S. Walton, Understanding DABCO Nanorotor Dynamics in Isostructural Metal-Organic Frameworks, J. Phys. Chem. Lett. 6 (5) (2015) 812–816.

[43] Y. Wu, Z. Liu, J. Peng, X. Wang, X. Zhou, Z. Li, Enhancing Selective Adsorption in a Robust Pillared-Layer Metal-Organic Framework via Channel Methylation for the Recovery of C2–C3 from Natural Gas, ACS Appl. Mater. Interfaces 12 (46) (2020) 51499–51505.

[44] S. Xing, J. Liang, P. Brandt, F. Schäfer, A. Nuhnen, T. Heinen, I. Boldog, J. Möllmer, M. Lange, O. Weingart, C. Janiak, Capture and Separation of SO2 Traces in Metal-Organic Frameworks via Pre-Synthetic Pore Environment Tailoring by Methyl Groups, Angew. Chem. Int. Ed. 60 (33) (2021) 17998–18005.

[45] M. Åhlén, E. Kapaca, D. Hedbom, T. Willhammar, M. Strømme, O. Cheung, Gas sorption properties and kinetics of porous bismuth-based metal-organic frameworks and the selective CO2 and SF6 sorption on a new bismuth trimesate-based structure UU-200, Microporous Mesoporous Mater. 329 (2022) 111548.

[46] P.-J. Kim, Y.-W. You, H. Park, J.-S. Chang, Y.-S. Bae, C.-H. Lee, J.-K. Suh, Separation of SF6 from SF6/N2 mixture using metal–organic framework MIL-100 (Fe) granule, Chem. Eng. J. 262 (2015) 683–690.

[47] Q. Ding, Z. Zhang, C. Yu, P. Zhang, J. Wang, X. Cui, C.-H. He, S. Deng, H. Xing, Exploiting equilibrium-kinetic synergetic effect for separation of ethylene and ethane in a microporous metal-organic framework, Sci. Adv. 6 (15) (2020) eaaz4322.